J|A|C|S
ARTICLES
Published on Web 07/17/2002

Resonance-Stabilized 1,2,3-Dithiazolo-1,2,3-dithiazolyls as Neutral π-Radical Conductors

Leanne Beer,[1a] Jaclyn L. Brusso,[1a] A. Wallace Cordes,[1b] Robert C. Haddon,[1c] Mikhail E. Itkis,[1c] Kristin Kirschbaum,[1d] Douglas S. MacGregor,[1a] Richard T. Oakley,*[,1a] A. Alan Pinkerton,[1d] and Robert W. Reed[1a]

Contribution from the Department of Chemistry, University of Waterloo, Waterloo, Ontario N2L 3G1, Canada, Department of Chemistry and Biochemistry, University of Arkansas, Fayetteville, Arkansas 72701, Department of Chemistry and Center for Nanoscale Science and Engineering, University of California, Riverside, California 92521-0403, and Department of Chemistry, University of Toledo, Toledo, Ohio 43606-3390

Received March 6, 2002

Abstract: Alkylation of the zwitterionic heterocycle 8-chloro-bis[1,2,3]dithiazolo[4,5-*b*:5′,4′-*e*]pyridine (ClBP) with alkyl triflates affords 8-chloro-4-alkyl-4*H*-bis[1,2,3]dithiazolo[4,5-*b*:5′,4′-*e*]pyridin-2-ium triflates [ClBPR][OTf] (R = Me, Et, Pr). Reduction of these salts with decamethylferrocene affords the corresponding ClBPR radicals as thermally stable crystalline solids. The radicals have been characterized in solution by cyclic voltammetry and EPR spectroscopy. Measured electrochemical cell potentials and computed (B3LYP/6-31G**) gas-phase disproportionation enthalpies are consistent with a low on-site Coulombic barrier *U* to charge transfer in the solid state. The crystal structures of ClBPR (R = Me, Et, Pr) have been determined by X-ray crystallography (at 293 K). All three structures consist of slipped π-stacks of undimerized radicals, with many close intermolecular S···S contacts. ClBPMe undergoes a phase transition at 93 K to a slightly modified slipped π-stack arrangement, the structure of which has also been established crystallographically (at 25 K). Variable-temperature magnetic and conductivity measurements have been performed, and the results interpreted in light of extended Hückel band calculations. The room-temperature conductivities of ClBPR systems ($\sigma_{RT} \approx 10^{-5}$ to 10^{-6} S cm^{-1}), as well as the weak 1D ferromagnetism exhibited by ClBPMe, are interpreted in terms of weak intermolecular overlap along the π-stacks. The latter is caused by slippage of the molecular plates, a feature necessitated by the steric size of the R and Cl groups on the pyridine ring.

Introduction

For over 30 years the development of organic conductors, both molecular and polymeric, has relied almost exclusively on the use of charge transfer (CT) to generate charge carriers.[2] Accordingly, conductive systems have required two components, i.e., a donor and an acceptor, although both can be incorporated into a single molecule.[3] Carriers can also be injected directly into an otherwise closed shell material using field effect doping.[4]

An alternative to the CT paradigm is to use neutral π-radicals as the building blocks for a single-component molecular material. A stacked array of radicals in a neutral radical conductor (NRC) would function like atoms in an elemental metal[5] and, on the basis of a simple band model of electronic structure, the bulk material should possess a half-filled energy band, as in elemental sodium. There are, however, several shortcomings to this model. First, any 1D half-filled energy band is prone to a Peierls instability; i.e., the radicals may associate into closed shell dimers.[6] Second, and perhaps more importantly, if dimerization can be suppressed, e.g., by steric bulk, the resulting low bandwidth *W*, coupled with the high on-site Coulomb repulsion *U* associated with a half-filled band, leads to a Mott insulating state.[7] Essentially the liberated spins are trapped on the radicals and, while interesting magnetic interactions can be observed,[8] conductivity remains low. Many examples of such materials, based on phenalenyl[9] frameworks

(1) (a) University of Waterloo. (b) University of Arkansas. (c) University of California. (d) University of Toledo.
(2) (a) Marsitzky, D.; Mullen, K. In *Advances in Synthetic Metals*; Bernier, P., Lefrant, S., Bidan, G., Eds.; Elsevier: New York, 1999; p 1. (b) Grossel, M. C.; Weston, S. C. *Contemp. Org. Synth.* **1994**, *1*, 317. (c) Williams, J. M.; Ferraro, J. R.; Thorn, R. J.; Carlson, K. D.; Geiser, U.; Wang, H. U.; Kini, A. M.; Whangbo, M.-H. *Organic Superconductors (Including Fullerenes)*; Prentice Hall: Upper Saddle River, NJ, 1992. (d) Ferraro, J. R.; Williams, J. M. *Introduction to Synthetic Electrical Conductors*; Academic Press: New York, 1987; p 25.
(3) Tanaka, H.; Okano, Y.; Kobayashi, H.; Suzuki, W.; Kobayashi, A. *Science* **2001**, *291*, 281.
(4) (a) Dodabalapur, A.; Katz, H. E.; Torsi, L.; Haddon, R. C. *Science* **1995**, *269*, 1560. (b) Garnier, F.; Hajlaoui, R.; Yassar, A.; Srivastava, P. *Science* **1994**, *265*, 1684. (c) Dagoto, E. *Science* **2001**, *293*, 2410. (d) Schön, J. H.; Kloc, Ch.; Batlogg, B. *Science* **2001**, *293*, 2342.
(5) (a) Haddon, R. C. *Nature* **1975**, *256*, 394. (b) Haddon, R. C. *Aust. J. Chem.* **1975**, *28*, 2333. (c) Haddon, R. C. *Aust. J. Chem.* **1975**, *28*, 2334.
(6) Peierls, R. C. *Quantum Theory of Solids*; Oxford University Press: London, 1953; p 108.
(7) Mott, N. F. *Metal-insulator Transitions*; Taylor and Francis: London, 1990.
(8) (a) Banister, A. J.; Bricklebank, N.; Lavendar, I.; Rawson, J. M.; Gregory, C. I.; Tanner, B. K.; Clegg, W.; Elsegood, M. R.; Palacio, F. *Angew. Chem., Int. Ed. Engl.* **1996**, *35*, 2533. (b) Fujita, W.; Awaga, K. *Science* **1999**, *286*, 261. (c) McManus, G. D.; Rawson, F. M.; Feeder, N.; van Duijn, J.; McInnes, E. J. L.; Novoa, J. J.; Burriel, R.; Palacio, F.; Oliete, P. *J. Mater. Chem.* **2001**, *11*, 1992.

10.1021/ja026118s CCC: $22.00

Chart 1

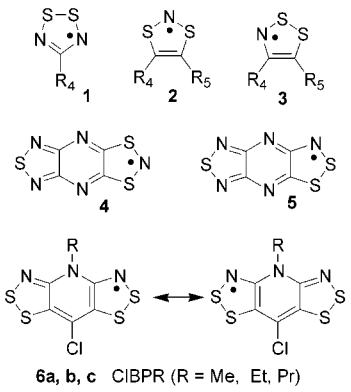

6a, b, c ClBPR (R = Me, Et, Pr)

and heterocyclic thiazyl/selenazyl skeletons,[10] have been characterized.

Improved conductivity thus requires the design of materials with a high *W*/*U* ratio, i.e., systems with a large bandwidth *W* and a small on-site repulsion *U*. While a priori estimation of the magnitude of both *W* and *U* is not practical, trends in the gas-phase disproportionation enthalpy ΔH_{disp}[11] for a series of related radicals provide a working mirror to the trends in *U*. For heterocyclic thiazyl radicals a limited database of experimentally obtained ionization potentials has been compiled,[12] and reliable estimates of both IP and EA values can now be easily obtained by computation.[13,14] Alternatively, solution-based cell potentials E_{cell}, which are generally accessible by experiment, can be used.[15] Using either criterion, the working prescription for NRCs requires radicals with good ion energetics, i.e., low ΔH_{disp} and E_{cell} values. In addition, the radicals must not dimerize in the solid state, and yet should exhibit a strong network of intermolecular interactions, so that sufficient electronic bandwidth is generated to offset the on-site Coulomb barrier *U*.

Much of our early work with NRCs focused on 1,2,3,5-dithiadiazolyl (DTDA) radicals **1** (Chart 1), but these materials suffered from rather large ΔH_{disp} and E_{cell} values regardless of the nature of the 4-substituent.[16] By contrast, the redox properties of 1,3,2- and 1,2,3-dithiazolyl (DTA) radicals **2** and **3** can be significantly modified by the electron-widthdrawing/releasing power of the 4,5-substituents. We have shown that while simple monofunctional derivatives have relatively large disproportionation energies, attachment of electron-withdrawing groups at the 4,5-positions, as in the tricyclic compounds **4** and **5**, leads to a significant reduction in ΔH_{disp}; experimental E_{cell} values follow suit. Structural analysis of **4** revealed an undimerized structure (at room temperature), but the spins remained isolated; i.e., the material was a Mott insulator.[17] By contrast, while molecules of **5** dimerize in the solid state, magnetic and conductivity measurements indicated that the free spins present as defects serve as charge carriers.[18]

While providing encouraging results, i.e., good ion energetics and a lower *U*, electron delocalization in compounds such as **4** and **5** arose from the attachment of a highly electron withdrawing substituent to an otherwise localized DTA radical (**2** or **3**). There are limits to this approach; e.g., is it useful, or even possible, to build an even more effective electron-withdrawing substituent? As an alternative design strategy we are now exploring radicals in which the extent of spin delocalization is enhanced by a resonance interaction between two DTA rings, one a 1,2,3-dithiazolyl radical and the other a closed shell 1,2,3-dithiazole. As an example of this hitherto unknown arrangement we have developed the *N*-alkylpyridine-bridged 1,2,3-dithiazolo-1,2,3-dithiazolyl framework ClBPR **6**. On the basis of the two equivalent resonance structures shown in Chart 1, such radicals should have highly delocalized spin distributions, and display ΔH_{disp} and E_{cell} values superior to those observed for conventional DTA-based π-radicals. Here we describe the preparation and the electrochemical, spectroscopic, and structural characterization of three ClBPR radicals (R = Me, Et, and Pr). Variable-temperature magnetic susceptibility and single-crystal conductivity measurements have also been performed. The results are discussed in light of the design criteria for NRC materials.

Results

Synthesis. 1,2,3-DTA radicals **3** have been known for many years,[19,20] but few examples have been isolated and structurally characterized; their thermal stability is extremely dependent on the nature of the 4,5-substituents.[21] Typically, the radicals are generated by reduction of salts of the corresponding closed shell 1,2,3-DTA cations, for which a variety of synthetic routes are known.[22] One of the most well-known approaches is via the

(9) For recent examples, see: (a) Koutentis, P. A.; Chen, Y.; Cao, Y.; Best, C. P.; Itkis, M. E.; Beer, L.; Oakley, R. T.; Cordes, A. W.; Brock, C. P.; Haddon, R. C. *J. Am. Chem. Soc.* **2001**, *123*, 3864. (b) Koutentis, P. A.; Haddon, R. C.; Oakley, R. T.; Cordes, A. W.; Brock, C. P. *Acta Crystallogr.* **2001**, *B57*, 680. (c) Goto, K.; Kubo, T.; Yamamoto, K.; Nakasuji, K.; Sato, K.; Shiomi, D.; Takui, T.; Kubota, M.; Kobayashi, T.; Yakusi, K.; Ouyang, J. *J. Am. Chem. Soc.* **1999**, *121*, 1619.

(10) For recent examples, see: (a) Beer, L.; Cordes, A. W.; Myles, D. J. T.; Oakley, R. T.; Taylor, N. J. *CrystEngComm* **2000**, 20. (b) Britten, J. F.; Clements, O. P.; Cordes, A.W.; Haddon, R. C.; Oakley, R. T.; Richardson, J. F. *Inorg. Chem.* **2001**, *40*, 6820. (c) Cordes, A. W.; Haddon, R. C.; Oakley, R. T. *Adv. Mater.* **1994**, *6*, 798. (d) Cordes, A. W.; Haddon, R. C.; Oakley, R. T. In *The Chemistry of Inorganic Ring Systems*; Steudel, R., Ed.; Elsevier: Amsterdam, 1992; p 295.

(11) ΔH_{disp} is the enthalpy change for the conversion of two gas-phase radicals R into a cation/anion pair, i.e., $2R \rightleftarrows R^+ + R^-$, and accordingly is equal to the difference between the ionization potential (IP) and electron affinity (EA). The solution-based cell potential $E_{cell} = E_{1/2}(ox) - E_{1/2}(red)$ is the difference between the half-wave potentials for the oxidation and reduction processes.

(12) (a) Boeré, R. T.; Oakley, R. T.; Reed, R. W.; Westwood, N. P. C. *J. Am. Chem. Soc.* **1989**, *111*, 1180. (b) Cordes, A. W.; Goddard, J. D.; Oakley, R. T.; Westwood, N. P. C. *J. Am. Chem. Soc.* **1989**, *111*, 6147. (c) Cordes, A. W.; Bryan, C. D.; Davis, W. M.; de Laat, R. H.; Glarum, S. H.; Goddard, J. D.; Haddon, R. C.; Hicks, R. G.; Kennepohl, D. K.; Oakley, R. T.; Scott, S. R.; Westwood, N. P. C. *J. Am. Chem. Soc.* **1993**, *115*, 7232. (d) Brownridge, S.; Du, H.; Fairhurst, S. A.; Haddon, R. C.; Oberhammer, Parsons, S.; Passmore, J.; Schriver, M. J.; Sutcliffe, L. H.; Westwood, N. P. C. *J. Chem. Soc., Dalton Trans.* **2000**, 3365.

(13) Kaszynski, P. *J. Phys. Chem. A* **2001**, *105*, 7626.

(14) Cordes, A. W.; Mingie, J. R.; Oakley, R. T.; Reed, R. W.; Zhang, H. *Can. J. Chem.* **2001**, *79*, 1352.

(15) Boeré, R. T.; Roemmele, T. L. *Coord. Chem. Rev.* **2000**, *210*, 369.

(16) (a) Boeré, R. T.; Moock, K. H. *J. Am. Chem. Soc.* **1995**, *117*, 4755. (b) Chandrasekhar, V.; Chivers, T.; Parvez, M.; Vargas-Baca, I.; Ziegler, T. *Inorg. Chem.* **1997**, *36*, 4772.

(17) Barclay, T. M.; Cordes, A. W.; George, N. A.; Haddon, R. C.; Itkis, M. E.; Mashuta, M. S.; Oakley, R. T.; Patenaude, G. W.; Reed, R. W.; Richardson, J. F.; Zhang, H. *J. Am. Chem. Soc.* **1998**, *120*, 352.

(18) Barclay, T. M.; Cordes, A. W.; Haddon, R. C.; Itkis, M. E.; Oakley, R. T.; Reed, R. W.; Zhang, H. *J. Am. Chem. Soc.* **1999**, *121*, 969.

(19) Preston, K. F.; Sutcliffe, L. H. *Magn. Reson. Chem.* **1990**, *28*, 189.

(20) (a) Mayer, R.; Domschke, G.; Bleisch, S. *Tetrahedron Lett.* **1978**, 4003. (b) Mayer, R.; Domschke, G.; Bleisch, S.; Bartl, A.; Stăsko, A.; *Z. Chem.* **1981**, *21*, 146, 264. (c) Mayer, R.; Domschke, G.; Bleisch, S.; Fabian, J.; Bartl, A.; Stăsko, A. *Collect. Czech. Chem. Commun.* **1984**, *49*, 684. (d) Mayer, R.; Bleisch, S.; Domschke, G.; Tráč, A.; Stăsko, A. *Org. Magn. Reson.* **1979**, *12*, 532. (e) Harrison, S. R.; Pilkington, R. S.; Sutcliffe, L. H. *J. Chem. Soc., Faraday Trans. 1* **1984**, *80*, 669.

(21) Barclay, T. M.; Beer, L.; Cordes, A. W.; Oakley, R. T.; Preuss, K. E.; Taylor, N. J.; Reed, R. W. *Chem. Commun.* **1999**, 531.

(22) (a) Rawson, J. M.; McManus, G. D. *Coord. Chem. Rev.* **1999**, *189*, 135. (b) Torroba, T. *J. Prakt. Chem.* **1999**, *341*, 99. (c) Kim, K. *Sulfur Rep.* **1998**, *21*, 147.

Scheme 1

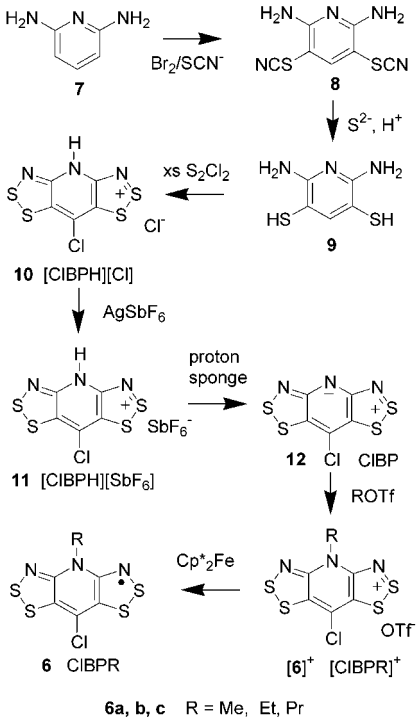

Herz reaction, i.e., the cyclocondensation of an aromatic amine with S_2Cl_2.[23] While we were eventually able to access the ClBPR framework using a variation of Herz technology, our initial attempts (Scheme 1) to produce a resonance-stabilized bis(1,2,3-DTA) radical started from the pyridine bis(aminothiol) **9**, itself prepared by a procedure developed for the analogous benzene compound, i.e., oxidative thiocyanation of 2,6-diaminopyridine **7** to the 3,5-bis(thiocyanate) **8**,[24] followed by hydrolysis.[25] Condensation of **9** with excess S_2Cl_2 in refluxing chlorobenzene then afforded the protonated salt [ClBPH][Cl] (**10**) as a black insoluble solid. This crude chloride salt could be converted by metathesis with $AgSbF_6$ into the corresponding hexafluoroantimonate [ClBPH][SbF_6] (**11**). The latter salt, which is stable in air, is very soluble in CH_3CN, and partially soluble in glacial acetic acid and SO_2(l), giving rise to intensely blue solutions. Recrystallization of **11** from SO_2(l) afforded lustrous golden blocks suitable for structural analysis.[26] Both **10** and **11** derive from the antiaromatic 16π-electron base ClBP (**12**), which, as expected from its zwitterionic formulation, is more basic than a typical pyridine heterocycle. Deprotonation of [ClBPH][SbF_6] could not therefore be effected with triethylamine, but Proton Sponge readily liberated the parent zwitterion.

The above sequence of reactions represents the method initially developed to construct the ClBP framework. Later, however, we discovered that the chloride salt **10** could be prepared *in a single step* with a "double Herz" reaction, i.e., by heating 2,6-diaminopyridine with excess S_2Cl_2 at reflux in dichloroethane (Scheme 2). However, while the yield of the material so produced was high, its purity was not as good as that generated by the route outlined in Scheme 1. It did not, for example, undergo a clean metathesis with $AgSbF_6$. The crude chloride salt could nonetheless be purified by reacting it with $GaCl_3$ in CH_3CN. This afforded the gallate salt [ClBPH][$GaCl_4$] (**13**), from which impurities could be removed by washing with glacial acetic acid (in which the gallate salt is insoluble). Reprecipitation of the chloride, by addition of pyridine to an acetonitrile solution of the gallate, gave material which underwent a very smooth metathesis with $AgSbF_6$ in CH_3CN to afford pure [ClBPH][SbF_6]. Subsequent treatment with Proton Sponge afforded ClBP in good overall yield.[27] This method is superior for large-scale preparations of ClBP.

Scheme 2

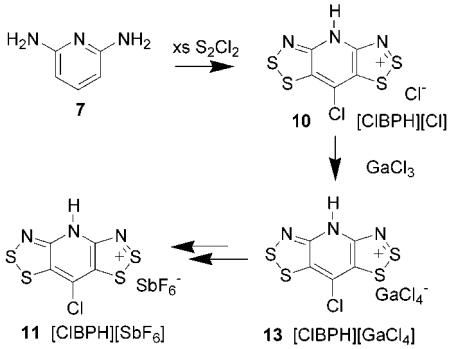

Regardless of how the free base ClBP was produced, the final step in the assembly of the ClBPR framework involved the conversion of ClBP into a series of N-alkylated derivatives [ClBPR]$^+$ (R = Me, Et, Pr). This was easily performed in diethyl ether using a slight excess of the appropriate alkyl triflate ROTf, although for R = Et and Pr prolonged reaction times were necessary. The triflates [ClBPR][OTf] (R = Me, Et, Pr) precipitated from solution as metallic red microcrystals which are stable in air and readily dissolve in acetonitrile to afford deep blue solutions. They were recrystallized for analytical purposes from glacial acetic acid.

The *N*-alkyl triflates [ClBPR][OTf] (R = Me, Et, Pr), along with the protonated salt [ClBPH][SbF_6], are based on 16π-electron frameworks which should, upon reduction, afford 17π-electron ClBPR radicals **6**. Preliminary attempts at chemical reduction were not, however, encouraging. For example, triphenylantimony, a reagent which has proven effective for reducing a wide range of 1,2,3-DTA cations, failed to react at all with any of the [ClBPR]$^+$ salts. Resolution of the problem required examination of the necessary electrochemical potentials. The results of such a study, described in the following section, indicated the need for a more powerful reducing agent; the properties of decamethylferrocene (Cp_2*Fe) (vide infra) suggested a perfect match.[28] To our satisfaction treatment of [ClBPR][OTf] (R = Me, Et, Pr) with 1 equiv of Cp_2*Fe in degassed CH_3CN afforded a metallic green/black microcrystalline precipitate of the corresponding ClBPR radical **6** in high yield (Scheme 1). The crude radicals were purified, for structural characterization and transport property measurements, by recrystallization from degassed $C_2H_4Cl_2$. In contrast to the

(23) (a) Herz, R. *Chem. Zentralbl.* **1922**, *4*, 948. (b) Warburton, W. K. *Chem. Rev.* **1957**, *57*, 1011.
(24) (a) Baker, A. J.; Hill, S. A. *J. Chem. Soc.* **1962**, 3464. (b) Lochon, P.; Méheux, P.; Néel, J. *Bull. Soc. Chim. Fr.* **1967**, *11*, 4387. (c) Okada M.; Marvel, C. S. *J. Polym. Sci., Part A-1* **1968**, *6*, 1259.
(25) Huestis, L. D.; Walsh, M. L.; Hahn, N. *J. Org. Chem.* **1965**, 2763.
(26) A preliminary account of the preparation and structural characterization of [ClBPH][SbF_6] and ClBP has been published. See: Beer, L.; Cordes, A. W.; Oakley, R. T.; Mingie, J. R.; Preuss, K. E.; Taylor, N. J. *J. Am. Chem. Soc.* **2000**, *122*, 7602.
(27) The gallate salt **13** could not be converted directly to **12**. Treatment of **13** with Proton Sponge led to partial decomposition of the $GaCl_4^-$ anion, and precipitiation of a mixture of **12** and **10**.
(28) Novriandi, I.; Brown, K. N.; Fleming, D. S.; Gulyas, P. T. Lay, P. A.; Masters, A. F.; Phillips, L. *J. Phys. Chem.* **1999**, *103*, 2713.

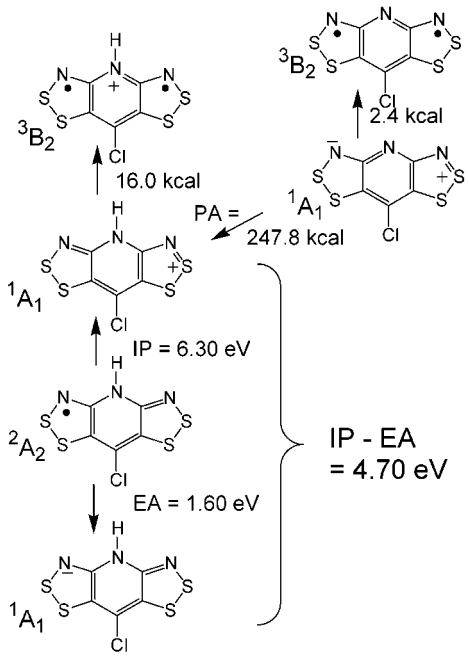

Figure 1. Calculated (B3LYP/6-31G**) gas-phase ion energetics for ClBP and $[ClBPH]^+$.

behavior of the alkylated salts, reduction of the protonated salt $[ClBPH][SbF_6]$ under the same conditions as those used for [ClBPR][OTf] (R = Me, Et, Pr) produced a black uncharacterized solid. This apparent anomaly was later rationalized in light of the cyclic voltammetric behavior (vide infra) of the $[ClBPH]^+$ cation.

Electronic Structure Calculations. We have explored the electronic structures and energies of several derivatives based on the ClBP and ClBPH frameworks by means of a series of density functional theory (DFT) calculations at the B3LYP/6-31G** level; the results are summarized in Figure 1. ClBP itself represents a rare (to our knowledge, the only) example of an antiaromatic sulfur nitrogen heterocycle with a zwitterionic ground state.[29] While both ClBP and its protonated variant $[ClBPH]^+$ are predicted to be closed shell species, the singlet $^1A_1$ ground state of ClBP lies only 2.4 kcal mol^{-1} below the $^3B_2$ diradical triplet (Figure 1); for $[ClBPH]^+$ the singlet/triplet splitting is much larger (16.0 kcal mol^{-1}). As expected from its dipolar formulation, ClBP is a relatively strong base; its calculated proton affinity (PA = 247.7 kcal mol^{-1}) is estimated to be very close to that of Proton Sponge (PA = 246 kcal mol^{-1}),[30] and it was on this basis that the latter base was selected for the deprotonation of $[ClBPH]^+$.

Sequential reduction of $[ClBPH]^+$ leads to the 17π-electron radical ClBPH and the 18π-electron anion $[ClBPH]^-$; computed (ΔSCF) IP and EA values for the radical are, respectively, 6.30 and 1.6 eV. Within the context of NRC design the resulting ΔH_{disp} of 4.70 eV represents a dramatic improvement on any previously studied 1,2,3-DTA radical; indeed it is comparable to that found for metallic elements, e.g., sodium.[31] As noted earlier the superior ion energetics of the ClBPH radical

(29) Hutchison, K.; Srdanov, G.; Hicks, R.; Yu, H.; Wudl, F.; Strassner, T.; Nendel, M.; Houk, K. N. *J. Am. Chem. Soc.* **1998**, *120*, 2989.
(30) Maier, J. P. *Helv. Chim. Acta* **1974**, *57*, 994.
(31) For sodium ΔH_{disp} = IP − EA = 5.14 − 0.55 = 4.59 eV. See: (a) Moore, C. E. *Natl. Stand. Ref. Data Ser. (U.S. Natl. Bur. Stand.)* **1970**, *34*, 1. (b) Hotop, H.; Lineberger, W. C. *J. Phys. Chem. Ref. Data* **1985**, *14*, 731.

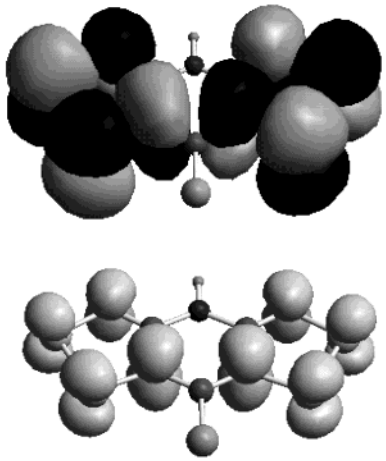

Figure 2. B3LYP/6-31G** SOMO (top) and spin density distribution (bottom) for ClBPH. Atomic spin densities are S(C) 0.120, S(N) 0.264, N(S) 0.170, C(S) 0.288, C(N) −0.086, and C(Cl) −0.167 (other atoms <0.02).

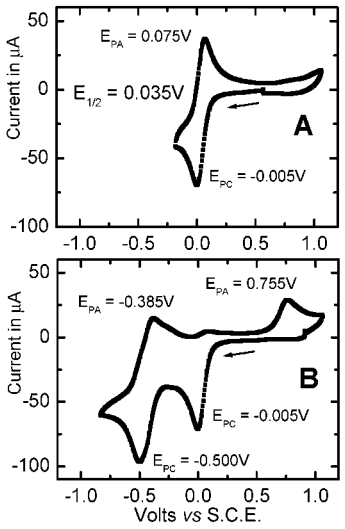

Figure 3. CV scans of $[ClBPH][SbF_6]$ in CH_3CN, [*n*-Bu_4N][PF_6] supporting electrolyte: (A) +1.0 to −0.25 V sweep and (B) +1.0 to −0.80 V sweep.

compared to monofunctional DTAs can be attributed, in valence bond parlance, to resonance between the two 1,2,3-DTA rings. The extent of spin delocalization can be more easily visualized in molecular orbital terms from the distribution of the a_2 SOMO (Figure 2), which is an out-of-phase combination of two 1,2,3-DTA SOMOs; derived total spin densities are also shown in Figure 2.

Cyclic Voltammetry. While the DFT calculations described above provide an encouraging picture of the ion energetics of the $[ClBPH]^+$ cation, examination of the electrochemical behavior of $[ClBPH][SbF_6]$ yielded unexpected results. A cyclic voltammetric (CV) sweep on an acetonitrile solution of this salt over the range +1.0 to −0.25 V vs SCE, with Pt wire electrodes and [Bu_4N][PF_6] as supporting electrolyte, revealed a single reversible reduction wave with $E_{1/2}$ = 0.035 V (Figure 3A). This we ascribe to the reduction of the $[ClBPH]^+$ cation to the ClBPH radical, i.e., the +1/0 couple. When the CV sweep range was extended to −0.8 V, a second, irreversible reduction process with a cathodic peak potential E_{pc} = −0.500 V was observed; this we assign to the 0/−1 couple. Reversal of the voltage sweep

Scheme 3

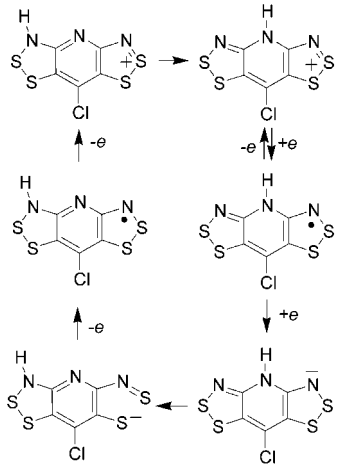

afforded an oxidation wave for the 0/−1 couple with peak potential $E_{pa} = -0.385$ V. At the same time the reversibility of the +1/0 couple process was lost, to be replaced by a single irreversible oxidation wave with $E_{pa} = 0.755$ V (Figure 3B). This dramatic change in the CV, occasioned simply by a change in sweep width, could be entirely reversed by returning to the original voltage sweep. Thus, a repeat CV scan over the range +1.0 to −0.25 V vs SCE afforded exactly the same results as seen initially, i.e., a single reversible process corresponding to $E_{1/2}$(ox) of ClBPH. These two scans were reproducible even after repeated cycling between the two voltage ranges.

This seemingly unusual behavior is the fingerprint of a system exhibiting electrochemical irreversibility with chemical reversibility (EI−CR).[15] The condition for EI−CR arises when a chemical change is occurring much faster than the cycling rate of the CV scan, as, for example, in the reduction of dithioles, which leads to S−S bond cleavage and formation of a sulfidothioketone.[15,32] In the present case the redox chemistry of ClBPH is perturbed by the migratory capability of the N−H proton. A possible, but by no means exclusive, interpretation of the structural changes that occur during the CV scan of [ClBPH][SbF_6] is shown in Scheme 3. Electrochemical reversibility of the +1/0 couple is possible as long as the cathodic sweep does not reach potentials that can generate the anion. If such a potential is reached, a rapid structural change occurs following the formation of the $[ClBPH]^-$ anion. The structural change is precipitated by a proton shift from the pyridine nitrogen to the DTA ring. There are other tautomers possible in addition to the one shown, but regardless of which, or how many, are involved, the net effect of anion formation is to produce a more localized electronic structure.[33] This is probably accompanied by cleavage of one of the S−S (or S−N)[34] bonds. In the anodic sweep oxidation of the rearranged anion to a radical, and of this radical to a cation, will take place at potentials quite different from those observed in the cathodic sweep. Presumably upon re-formation of the cation, a proton shifts back to the pyridine nitrogen to regenerate the original $[ClBPH]^+$ framework.

(32) Bechgaard, K.; Parker, V. D.; Pedersen, C. T. *J. Am. Chem. Soc.* **1973**, *95*, 4373.
(33) In most monofunctional 1,2,3-DTAs the 0/−1 couple is irreversible.
(34) Alternatively N−S bond cleavage could occur. See, for example: Barclay, T. M.; Cordes, A. W.; Goddard, J. D.; Mawhinney, R. C.; Oakley, R. T.; Preuss, K. E.; Reed, R. W. *J. Am. Chem. Soc.* **1997**, *119*, 12136.

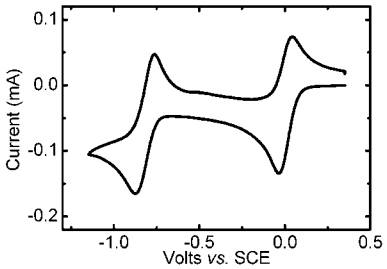

Figure 4. CV scan of [ClBPMe][OTf] in CH_3CN, [*n*-Bu_4N][PF_6] supporting electrolyte.

Table 1. Half-Wave Redox[a] and Cell Potentials[b]

	ClBPH	ClBPMe	ClBPEt	ClBPPr
$E_{1/2}$(ox) (V)	0.035	0.005	−0.018	−0.0116
$E_{1/2}$(red) (V)	*c*	−0.835	−0.845	−0.834
E_{cell} (V)		0.830	0.827	0.822

[a] In CH_3CN, reference to SCE. [b] $E_{cell} = E_{1/2}(ox) - E_{1/2}(red)$. [c] Irreversible behavior; see the text.

As expected from the above interpretation of the CV behavior of the $[ClBPH]^+$ system, replacement of the N−H proton by a nonmigratory alkyl group, as in the $[ClBPR]^+$ cations (R = Me, Et, Pr), eliminates the tautomerism issue, and produces far more straightforward electrochemistry. Using voltage ranges of +1.2 to −1.2 V vs SCE, cyclic voltammetry of all three [ClBPR][OTf] salts showed two reversible waves corresponding to the +1/0 and 0/−1 couples; the CV scan of [ClBPMe][OTf] in Figure 4 is representative. Analyses of the half-wave and E_{cell} values provided in Table 1 allow two important conclusions. (i) The +1/0 couple occurs at a potential far more anodic than that observed for monofunctional 1,2,3-DTA derivatives; i.e., ClBPR radicals are more powerful reducing agents. Generation of the radicals from the cations on a synthetic scale (vide supra) required a chemical reducing agent with sufficient potential to produce the radical state ClBPR but not the anion $[ClBPR]^-$, i.e., a redox couple within the range of 0 to −0.8 V vs SCE; to this end we selected decamethylferrocene, for which $E_{1/2}^{(0/+1)} = -0.13$ V.[28] (ii) The cell potentials E_{cell} for ClBPR radicals are near 830 mV, a value far smaller than the previous best (for two reversible couples), namely, the 1,2,3-DTA system **5**, for which $E_{cell} = 0.97$ V. These results, coupled with the gas-phase-computed ΔH_{disp} value of the parent ClBPH radical, provide compelling evidence for believing that in the solid state ClBPR radicals should enjoy a much lower on-site Coulomb repulsion *U* than any previously reported heterocyclic NRC.

EPR Spectra. We have been unable to observe any EPR spectrum for ClBPH, e.g., by in situ reduction of [ClBPH][SbF_6]. Calculated (B3LYP/6-31G**) *a* values for this species are provided in Table 2, and provide a satisfying cross match[35] with those observed experimentally for the N-alkylated radicals. The X-band EPR spectra of ClBPR (R = Me, Et, Pr) have been recorded at 293 K on CH_2Cl_2 solutions. The spectrum of ClBPMe shown in Figure 5 is representative; *g* values and hyperfine coupling constants are listed in Table 2. The spectra are characterized by a five-line pattern arising from spin coupling to the two equivalent ^{14}N nuclei on the two DTA rings. As expected from the fact that the spin density is partitioned equally between the two rings, a_N is much smaller than in monofunctional 1,2,3-DTAs. Smaller coupling to the pyridine

(35) Kaszynski, P. *J. Phys. Chem. A* **2001**, *105*, 7615.

Table 2. EPR Hyperfine Coupling Constants (mT) and *g* Values

		ClBPH[a]	ClBPMe	ClBPEt	ClBPPr
N(S)	a_N	0.346	0.310	0.310	0.310
N(R)	a_N	−0.066	0.060	0.060	0.060
Cl	a_{Cl}	−0.052	0.030/0.024[b]	0.030/0.024[b]	0.030/0.024[b]
$H(CH_2)$	a_H		0.030	<0.020	<0.020
H(X = H)[c]	a_H		0.30		
g value			2.008274	2.008208	2.008209

[a] B3LYP/6-31G** values from a C_{2v} geometry optimization; the single a_{Cl} value refers to the ^{35}Cl isotope. [b] The two a_{Cl} values correspond to the $^{35/37}$Cl isotopes, respectively. [c] Where R = CH_2X. Thus, X = H for R = Me and X = Me and Et for R = Et and Pr, respectively.

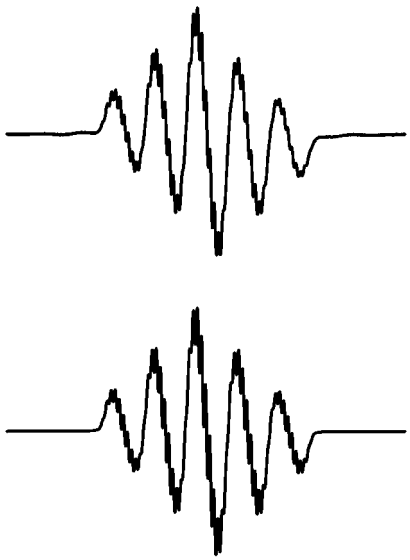

Figure 5. EPR spectrum of ClBPMe in CH_2Cl_2 (top) and simulation (bottom). SW = 3.0 mT, L/G ratio 0.50, and LW = 0.023 mT.

nitrogen, and to the basal chlorine, can be extracted by spectral simulation. ClBPMe also shows a small, equivalent coupling to the three methyl protons. No coupling is discernible to the methylene protons in either ClBPEt or ClBPPr.[36]

Crystal Structures. In the solid state the ClBPR radicals (R = Me, Et, Pr) are remarkably stable in air, but in solution they all decompose rapidly by reaction with dissolved oxygen. Crystals (green-black needles) of all three compounds suitable for X-ray analysis could nonetheless be obtained by recrystallization from carefully degassed (five freeze−pump−thaw cycles) toluene or dichloroethane. Crystals of ClBPMe could also be obtained by slow vacuum sublimation at 120 °C/10^{-3} Torr. Crystals of ClBPEt and ClBPPr are isomorphous, and belong to the tetragonal space group $P\bar{4}2_1m$, while those of ClBPMe belong to the orthorhombic space group $P2_12_12_1$. Magnetic measurements (vide infra) revealed a phase change for ClBPMe near 93 K, as a result of which its crystal structure has been determined both above (293 K = ClBPMe-RT) and below (25 K = ClBPMe-LT) this temperature. Crystal data for all structural determinations are listed in Table 3, and summaries of pertinent intramolecular bond lengths and intermolecular contacts compiled in Table 4. Packing diagrams are provided in Figures 6−9.

Crystals of ClBPEt and ClBPPr consist of slipped π-stacks of undimerized radicals running parallel to *z*. As such they represent the first examples of undimerized 1,2,3-DTA radicals.[18,21] Figure 6 shows the packing of ClBPEt stacks viewed down the *z* axis, and illustrates the clustering of the dithiazole heads about the $\bar{4}$ center. The ClBPMe structure (both phases) also consists of slipped π-stacks of undimerized radicals, although now the stacking direction is along *x* (Figure 7).

In the low-temperature phase ClBPMe-LT the *b* and *c* cell dimensions are shorter than in the room-temperature phase ClBPMe-RT, while the *a* axis is lengthened. At the molecular level this lateral compression and longitudinal elongation lead to the mean plane of the radicals in ClBPMe-LT being more sharply inclined (a decrease in the tilt angle τ) to the stacking axis than in ClBPMe-RT; the mean plane separation δ also contracts. This decrease in δ is, we believe, the driving force for the phase transition. In the absence of change in the tilt angle τ a general, and relatively uniform, contraction of all structural parameters (concomitant with a decrease in the cell constants *a*, *b*, and *c*) is normally observed on cooling. Such a process would, however, inevitably lead to closer Cl···Cl and Me···Me interactions, which are equal to the unit cell translation *a*. Avoiding such interactions, while still bringing the molecular planes closer together, requires an increase rather than a decrease in *a*, and this can only be brought about (if the space group is to be preserved) by a decrease in τ (a sharper tilt). In essence the phase change from ClBPMe-RT to ClBPMe-LT is reminiscent of the closing of venetian blinds.

In all three ClBPR structures there are numerous close intermolecular S···S contacts d1−d4 between neighboring dithiazole rings, about the $\bar{4}$ center in ClBPEt/Pr (Figure 8) and the 2_1 axes in ClBPMe (Figure 9). Most of these contacts are inside the van der Waals contact for sulfur (3.6 Å),[37] and some of those in the ClBPMe, notably d2 and d3, are among the shortest nonbonded S···S contacts that we have ever observed in an undimerized heterocyclic sulfur−nitrogen radical.

At the molecular level the bond lengths in all three radicals show classical trends relative to those seen in, for example, the oxidized ring of [ClBPH][SbF_6].[26] Occupation of the antibonding SOMO (Figure 2) leads to a general elongation of the S−S, S−N, and S−C bonds, but the changes are smaller than those seen between monofunctional DTA radicals and their cations, where the SOMO is localized over a single DTA ring,[21] and comparable to those seen between closed shell benzobis(dithiazoles) and their radical cations.[38]

Magnetic and Conductivity Measurements. Variable-temperature magnetic susceptibility (χ) measurements have been carried out on microcrystalline samples of ClBPR (R = Me, Et, Pr). The temperature dependence of χ for ClBPEt and ClBPPr shows normal Curie−Weiss[39] behavior for an $S = {}^1/_2$ system between 5 and 300 K; values of χ_0, *C*, and Θ are provided in Table 5. For ClBPMe, the temperature dependence of χ exhibits Curie−Weiss behavior from ambient temperatures down to 93 K (Figure 10), whereupon a hysteretic phase change occurs, leading to an increase in χ. Plots of the function χT vs *T* for the three compounds are shown, for comparative purposes,

(36) A B3LYP/6-31G** calculation on ClBPMe in C_s symmetry afforded a_H values of −0.095 mT for the single axial methyl proton, and −0.032 mT for the two equivalent gauche methyl protons. The observed a_H represents a time-averaged value for a freely rotating methyl group. In the case of ClBPEt and ClBPPr the methylene groups are locked with the two hydrogens in gauche positions, so that no coupling is observed.

(37) Bondi, A. *J. Phys. Chem.* **1964**, *68*, 441.
(38) (a) Barclay, T. M.; Cordes, A. W.; Oakley, R. T.; Preuss, K. E.; Reed, R. W. *Chem. Mater.* **1999**, *11*, 164. (b) Barclay, T. M.; Cordes, A. W.; Mingie, J. R.; Oakley, R. T.; Preuss, K. E. *Cryst. Eng. Chem.* **2000**, 15.
(39) Carlin, R. L. *Magnetochemistry*; Springer-Verlag: New York, 1986.

Table 3. Crystallographic Data

	ClBPMe-RT	ClBPMe-LT	ClBPEt	ClBPPr
empirical formula	$C_6H_3N_3ClS_4$	$C_6H_3N_3ClS_4$	$C_7H_5N_3ClS_4$	$C_8H_7N_3ClS_4$
fw	280.80	280.80	294.83	308.86
a, Å	4.2464(12)	4.5386(4)	15.886(4)	15.9601(19)
b, Å	15.194(5)	14.2658(10)	15.886(4)	15.9601(19)
c, Å	15.069(4)	14.3779(11)	4.1088(11)	4.4494(6)
V, Å^3	972.2(5)	930.92(13)	1036.9(5)	1133.4(2)
ρ(calcd), g cm^{-3}	1.918	2.004	1.889	1.810
space group	$P2_12_12_1$	$P2_12_12_1$	$P\bar{4}2_1m$	$P\bar{4}2_1m$
Z	4	4	4	4
temp, K	293(2)	25(5)	293(2)	293(2)
μ, mm^{-1}	1.208	1.261	1.137	1.045
λ, Å	0.71073	0.71073	0.71073	0.71073
no. of data/restraints/params	1915/0/128	1657/0/127	1064/0/87	700/0/82
solution method	direct methods	direct methods	direct methods	direct methods
R, R_w (on F^2)[a]	0.0314, 0.0544	0.0493, 0.1063	0.0279, 0.0571	0.0308, 0.0453

[a] $R = [\sum||F_o| - F_c||]/[\sum|F_o|]$ for $I > 2\sigma(I)$; $R_w = \{[\sum w||F_o|^2 - |F_c|^2|^2]/[\sum(w|F_o|^4)]\}^{1/2}$.

Table 4. Summary of Intra- and Intermolecular Structural Parameters

	ClBPMe-RT	ClBPMe-LT	ClBPEt	ClBPPr
temp (K)	293(2)	25(5)	293(2)	293(2)
Intramolecular Distances (Å)[a]				
S−S	2.101(6)	2.110(7)	2.1049(12)	2.1066(18)
S−N	1.661(7)	1.671(5)	1.663(3)	1.661(4)
S−C	1.731(8)	1.738(6)	1.728(3)	1.724(4)
N(S)−C	1.303(5)	1.309(9)	1.300(4)	1.300(4)
C(S)−C(N)	1.438(5)	1.435(28)	1.439(4)	1.428(5)
C(S)−C(Cl)	1.377(5)	1.380(19)	1.382(3)	1.387(4)
C−N(R)	1.385(14)	1.382(7)	1.382(3)	1.398(5)
Intermolecular Contacts[b] (Å) and Tilt Angles (deg)				
d1	3.541(2)	3.570(2)	3.742(1)	3.819(2)
d2	3.324(2)	3.234(2)	3.573(1)	3.505(2)
d3	3.369(2)	3.283(2)	3.560(1)	3.634(2)
d4	3.546(2)	3.449(2)	3.401(1)	3.563(2)
τ[c]	54.81(13)	48.73(12)	57.9(3)	51.0(3)
δ[d]	3.470(5)	3.411(8)	3.483(12)	3.458(9)

[a] Bond lengths in ClBPMe are an average of two values; numbers in parentheses are the larger of the ESD or the range. [b] See Figures 6−9 for definitions of d1−d4. [c] τ is the tilt angle between the mean molecular plane and the stacking axis. [d] δ is the mean interplanar separation between radicals along the π-stack.

in Figure 11. At ambient temperatures all three compounds exhibit values of χT near or slightly below 0.375 (the expected value for an $S = {}^1/_2$ system). The low-temperature "tails" in ClBPPr and ClBPEt herald, respectively, the onset of weak antiferromagnetic and ferromagnetic interactions. In ClBPMe, the phase change at 93 K can now be observed more clearly, as can the low-temperature antiferromagnetic tail below 14 K. The enhanced χT values between 14 and 93 K are characteristic of weak 1D ferromagnetic interactions along the π-stacks.[40,41]

Electrical conductivity (σ) measurements along the needle axes of ClBPR (R = Me, Et, Pr) were performed over the temperature range 150−330 K; Figure 12 shows log plots of σ against $1/T$ for the three compounds. As can be seen the conductivity is activated, with values of σ at 300 K increasing progressively from near 10^{-6} S cm^{-1} for R = Pr to 10^{-5} S cm^{-1} for R = Me (Table 5). The derived activation energies E_g (half of the band gap for an intrinsic semiconductor) steadily diminish from 0.48 (R = Pr) to 0.43 (R = Et) to 0.40 (R = Me) eV.

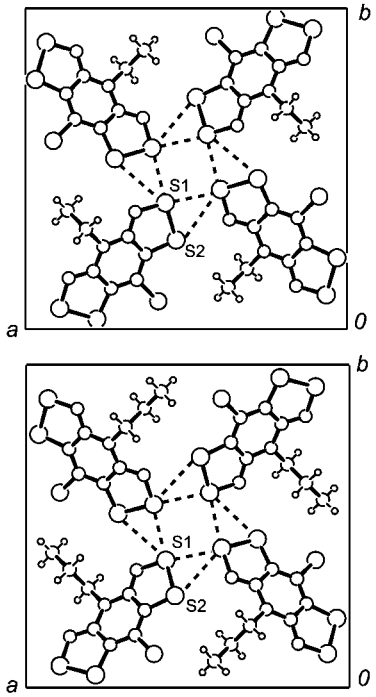

Figure 6. A projection of the packing of ClBPEt (top) and ClBPPr (bottom) in the *xy* plane. Intermolecular S···S contacts (dashed lines) are defined in Figure 8 and Table 4.

Band Structure Calculations. To place the above structural, magnetic, and conductivity results in context, we have performed a series of extended Hückel theory (EHT) band calculations on the four crystal structures under consideration, ClBPMe (LT and RT), ClBPEt, and ClBPPr. The results must be viewed with caution, as the EHT method cannot be expected to succeed in systems where the tight-binding approximation fails, i.e., in Mott insulators. The results are summarized in Figure 13, which shows the dispersion curves along the stacking direction[42] for the four crystal orbitals (COs) arising from the SOMOs of the four radicals in the unit cell, i.e., the putative half-filled conduction band of the molecular metal. Clearly, none of the materials is metallic, but the dispersion curves nonetheless provide insight into the extent of the intermolecular interactions along and perpendicular to the slipped π-stacks.

(40) (a) Lang, A.; Pei, Y.; Ouahab, L.; Kahn, O. *Adv. Mater.* **1996**, *8*, 60. (b) Kahn, O. *Molecular Magnetism*; VCH: New York, 1993.
(41) The magnetic properties of the ClBPR series will be discussed in more detail elsewhere.
(42) In all four structures $\alpha = \beta = \gamma = 90°$. There is therefore an exact equivalence of the directions of the unit cell vectors of the real and reciprocal space.

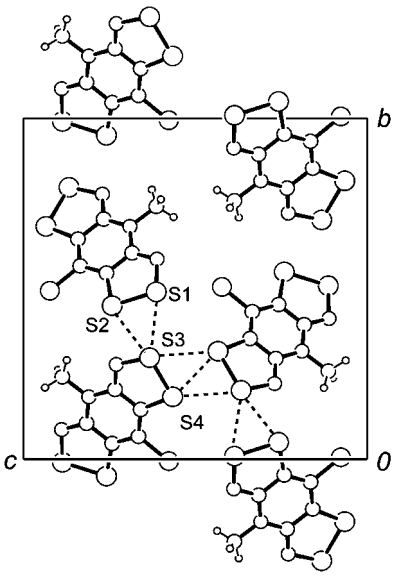

Figure 7. A projection of the packing of ClBPMe-RT in the *yz* plane. Intermolecular S···S contacts (dashed lines) are defined in Figure 9 and Table 4.

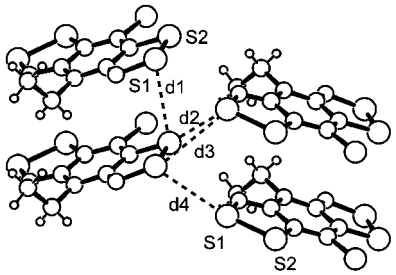

Figure 8. Side view of slipped π-stacks in ClBPEt, showing intermolecular S···S contacts d1−d4 (see Table 4). The ClBPPr structure is isomorphous.

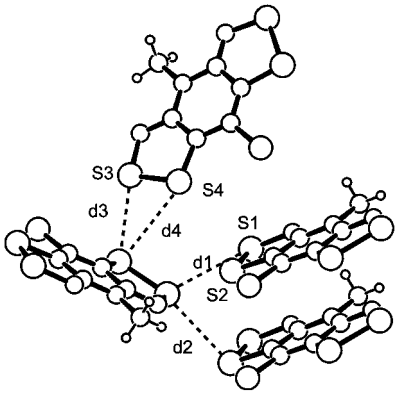

Figure 9. Side view of slipped π-stacks in ClBPMe-RT, showing intermolecular S···S contacts d1−d4 (see Table 4).

There are several salient features in Figure 13. (i) The slope of the curves, i.e., the sign of dE/dk, for ClBPEt and ClBPPr is the reverse of that seen in ClBPMe. (ii) Dispersion along the stack in ClBPPr and ClBPEt is approximately the same as, if not somewhat greater than, that observed in ClBPMe, in the region of 0.3−0.4 eV depending on the CO. The progressively increasing bandwidth along the series R = Pr, Et, and Me arises from the onset of lateral dispersion (the spreading of the four COs) in the latter. (iii) ClBPMe is a remarkably isotropic structure; lateral interactions appear to be as strong as those along the stack. The phase change from ClBPMe-RT to ClBPMe-LT is accompanied by an expected increase in dispersion both along and across the stack, but the ratio remains about the same. The interpretation of these findings is developed below.

Table 5. Magnetic Susceptibility[a] and Conductivity Data

	ClBPMe	ClBPEt	ClBPPr
χ_0, emu mol^{-1}	-137.5×10^{-6}	-160.0×10^{-6}	-162.4×10^{-6}
C, emu mol^{-1}	0.357[b]	0.326	0.349
Θ, K	−13[b]	7	−11.5
σ(300 K), S cm^{-1}	5.4×10^{-6}	3.2×10^{-6}	4.0×10^{-7}
E_g,[c] eV	0.395	0.43	0.48

[a] C and Θ obtained from the Curie−Weiss fits, i.e., χ = C/(T − Θ). [b] From a Curie−Weiss fit to data above 93 K. [c] E_g corresponds to the activation energy of the conductivity; for an intrinsic semiconductor and temperature-independent mobility, the band gap is twice this value.

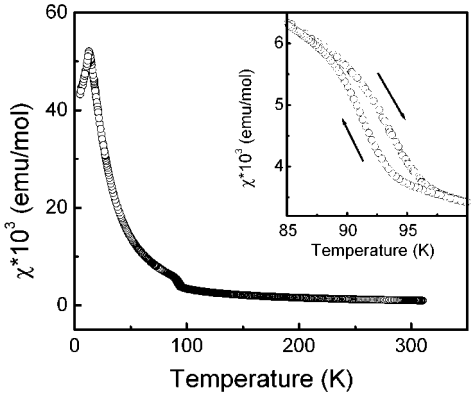

Figure 10. Magnetic susceptibility χ of ClBPMe as a function of temperature.

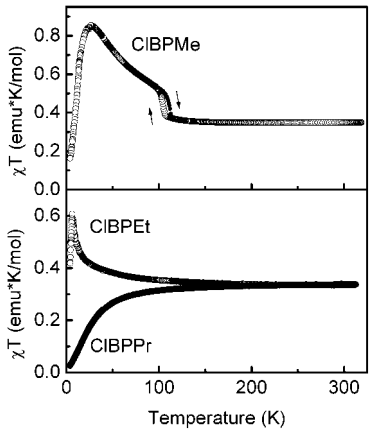

Figure 11. Temperature dependence of χT for ClBPMe (top) and ClBPEt and ClBPPr (bottom).

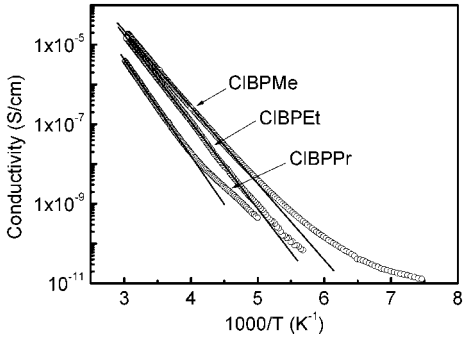

Figure 12. Log plots of σ vs 1/T for ClBPR (R = Me, Et, Pr).

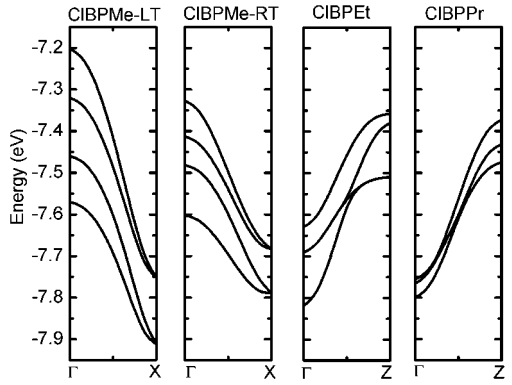

Figure 13. EHT dispersion curves for ClBPR radicals.

Discussion

On the basis of computed ion energetics and electrochemical data, the ClBPR system represents a major advance in the design of NRC materials. It provides a chemically robust framework which should, in the solid state, afford a much lower value of *U* than in other heterocyclic radicals. The observation of good conductivity requires, however, a large *W*/*U* ratio, i.e., strong intermolecular interactions and a large electronic bandwidth *W*. In the absence of the latter, a Mott insulating state will still prevail, regardless of the presence of favorable ion energetics. The relatively low room-temperature conductivities ($\sigma_{RT} \approx 10^{-5}$ to 10^{-6} S cm^{-1}) within the ClBPR series point to such a situation. The observation of 1D ferromagnetism in ClBPMe is also, we believe, a reflection of the narrow bandwidth of the material.

The origins of this problem, the failure to generate strong overlap between adjacent radicals along the π-stack and the consequently small value of *W*, can be traced back to the molecular shape of ClBPR radicals. Thus, while the cyclic framework is flat, the presence of the *N*-alkyl group and the chlorine atom *trans* to it create a sterically bulky "belt" which prevents direct superposition (and dimerization) of the radicals. Slippage of the radical stacks can occur along one of two directions (Figure 14); examples of each are found in the ClBPR structures. In ClBPMe the radicals slide sideways, perpendicular to the Cl···NR direction, while in ClBPEt and ClBPPr, they slide parallel to the Cl···NR direction. Within the context of the band structure calculations, these two motions lead to dramatically different types of overlaps between the SOMOs of adjacent rings. In the ClBPEt/Pr pair, the slippage is sufficient to remove all possible interactions save those between the two sets of S1···S2′ atoms (separated by d1). The in-phase combination of SOMOs in this arrangement (i.e., $k = 0$) is *bonding*, the reverse of that normally found for pπ−pπ overlap, and this leads to the seemingly anomalous π-type dispersion ($dE/dk > 0$) seen in Figure 13. The total dispersion is small, less than 0.5 eV, and is a direct result of the long d1 values (Table 4); a Mott insulating state follows.

In the case of ClBPMe, sideways slippage (Figure 14) seems, at first glance, to retain a reasonable opportunity for interaction between adjacent molecules; the close plane-to-plane separation δ (3.470 Å in the RT phase and 3.411 Å in the LT phase) certainly suggests so. In the absence of any short S···S or S···N contacts, the most plausible combinations for good overlap are between the two sulfurs of one DTA ring and a carbon atom[43] of its neighbor. These two S···C overlaps are, however, of *opposite* sign, so that the net effect is minimal. The longitudinal dispersion seen in ClBPMe (both phases) should therefore be viewed as arising from minor differences in the two S···C overlaps, and some small C···C overlaps. The combined interaction remains weak.[44]

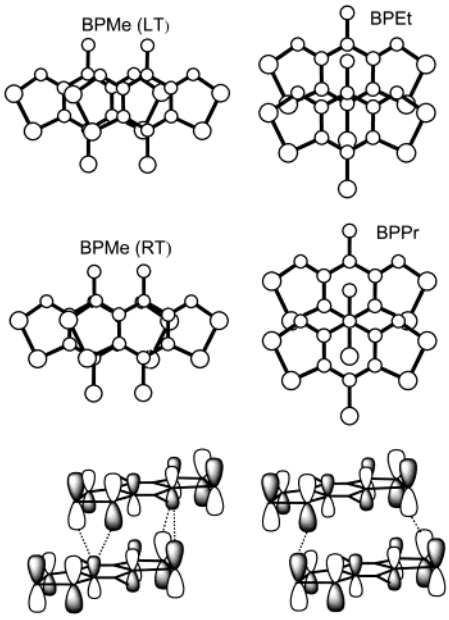

Figure 14. Projections of planes of nearest-neighbor rings in ClBPR structures (only the C_1 carbon of the R group is shown). Shown at the bottom are sketches of the SOMO overlaps in ClBPMe-LT/RT (left) and ClBPEt/Pr (right).

The trends in σ_{RT} values and activation energy gaps are in accord with the trends in EHT bandwidths, but the improved bandwidth in ClBPMe is largely a result of improved lateral interactions. The effective orthogonality of the S···C interactions, and the resulting poor overlap along the π-stacks in ClBPMe, also provide a simple orbital rationale for the weak 1D ferromagnetism in this compound. The observation of this phenomenon in organic (nonmetal-containing) structures is not common, but in metal-based systems the onset of ferromagnetism is often associated with an orthogonal orbital effect.[45]

Summary

Our pursuit of stable heterocyclic π-radicals suitable for NRC materials evolved from attempts to generate perfectly superimposed π-stacked assemblies of DTDA **1** radicals.[10] While such materials were thermally very stable, their electronic structures were extremely 1D, and in the absence of steric constraints spin-pairing dimerization was inevitable. Even when intradimer bonds were ruptured, i.e., at elevated temperatures, the liberated spins were not charge carriers; the free electrons were trapped on the radical centers, resulting in a Mott insulating state. In an attempt

(43) There are two carbons in each 1,2,3-DTA ring; the ClBPR radical SOMO (Figures 2 and 14) is almost nodal at one of these.
(44) To assess what a strong interaction might be, we carried out a model dispersion calculation on a 1D stack of perfectly superimposed ClBPH radicals (with Cl replaced by H to avoid steric problems) set 3.45 Å apart. The resulting dispersion was 2.5 eV, much larger than that seen in any of the present ClBPR structures.
(45) (a) Landrum G. A.; Dronkowski, R. *Angew. Chem., Int. Ed.* **2000**, *39*, 1560. (b) Verdaguer, M. *Polyhedron* **2001**, *20*, 1115. (c) Hicks, R. G.; Lemaire, M. T.; Richardson, J. R.; Thompson, L. K.; Xu, Z. *J. Am. Chem. Soc.* **2001**, *123*, 7154. (c) Manson, J. L.; Arrif, A. M.; Miller, J. S. *Chem. Commun.* **1999**, 1479.

to overcome the Mott insulator problem, more delocalized radicals such as the fused ring 1,3,2-DTA and 1,2,3-DTA derivatives **4** and **5** were developed.[17,18] These exhibited improved ion energetics and conductivities. However, while the crystal structures of compound **4**[17] and related compounds[8b,c] consist of undimerized slipped π-stacks at ambient temperatures, they too exhibit a propensity to slide into spin-paired dimers at low temperatures. The possibility of utilizing these phase changes in magnetic switching devices has been suggested.[8b,c]

Highly delocalized dithiazolodithiazolyl radicals, of which the ClBPR series (R = Me, Et, Pr) described here are the first examples, constitute a new generation of molecular building blocks with potential applications in single-component magnetic and conductive materials. Their calculated gas-phase disproportionation enthalpies and measured electrochemical cell potentials are superior to those of all previously known heterocyclic radicals, and should afford materials with a low on-site repulsion *U*. However, while the Cl and R groups in the sterically bulky "belt" prevent dimerization, they also militate against well-developed electronic band dispersion along the π-stack. The paramagnetic to weakly 1D ferromagnetic phase transition at 93 K in ClBPMe is a manifestation of this weak bandwidth *W*. Interestingly, and in contrast to the phase changes observed for DTDA and DTA radicals, the structural change associated with this phase transition in ClBPMe involves an adjustment to a more (rather than less) acutely slipped π-stack array. We are currently pursuing variants of the dithiazolodithiazolyls described here, derivatives in which the exocyclic substituents are either modified or removed entirely. Larger *W*/*U* ratios and improved conductivities will hopefully follow.

Experimental Section

General Procedures and Starting Materials. The reagents 2,6-diaminopyridine, ammonium thiocyanate, bromine, sodium sulfide hydrate, sulfur monochloride, gallium trichloride, silver hexafluoroantimonate, Proton Sponge, methyl and ethyl triflates, and decamethylferrocene were obtained commercially (all from Aldrich) and used as received. Sulfur dioxide gas (reagent grade, Matheson) was also used as received. Propyl triflate[46] was prepared according to literature methods. All solvents were of at least reagent grade, and dried by distillation from P_2O_5 (for acetonitrile, chlorobenzene, and dichloroethane). All reactions were performed under an atmosphere of dry nitrogen. Melting points are uncorrected. Infrared spectra (Nujol mulls, KBr optics) were recorded on a Nicolet Avatar FTIR spectrometer at 2 cm^{-1} resolution. Low-resolution mass spectra (70 eV, EI/DEI and CI/DCI) were run on a Finnigan 4500 quadrupole mass spectrometer at the McMaster Regional Centre for Mass Spectrometry. Elemental analyses were performed by MHW Laboratories, Phoenix, AZ.

Preparation of 2,6-Diaminopyridine-3,5-bis(thiocyanate), 8. A solution of Br_2 (19.0 mL, 0.358 mol) in 100 mL of methanol was added dropwise over 30 m to a stirred solution of 2,6-diaminopyridine (10.0 g, 0.092 mol) and ammonium thiocyanate (56.0 g, 0.736 mol) in 400 mL of methanol. The reaction mixture was kept on ice until the addition was complete and then allowed to stir at room temperature for 1 h to afford a white precipitate. The mixture was poured onto 1 L of ice/water and left for 1 h. The resulting gray precipitate was collected by filtration, washed with 3 × 100 mL of water, and dried in air. The product **8** was recrystallized from hot glacial acetic acid as yellow crystals; yield 14.1 g (0.063 mol, 68%), mp > 200 °C dec. IR: 3494 (m), 3429 (m), 3381 (m), 3325 (w), 3140 (m, br), 2152 (s), 1659 (s), 1629 (s), 1601 (s), 1561 (s), 1540 (s), 1249 (w), 953 (w), 756 (m), 663 (w), 573 (w), 490 (m), 458 (w) cm^{-1}. ^1H NMR (δ, DMSO): 7.87 (s, aromatic), 6.95 (s, amino). MS (*m*/*e*): 223 (M^+, 48), 197 ([M − CN]$^+$, 10), 165 ([M − SCN]$^+$, 86). Anal. Calcd for $C_7H_5N_3S_5$: C, 37.65; H, 2.26; N, 31.37. Found: C, 37.65; H, 2.18; N, 31.42.

Synthesis of 2,6-Diaminopyridine-3,5-dithiol, 9. A slurry of 2,6-diaminopyridine-3,5-bis(thiocyanate) (1.99 g, 8.93 mmol) and sodium sulfide nonahydrate (8.74 g, 36.4 mmol) was warmed in 90 mL of degassed, deionized water for 1 h. The brown-yellow solution was cooled on ice, and to this was added glacial acetic acid, dropwise, until a pH of 5.5−6.0 was attained. The mixture was stirred for 30 min and the yellow precipitate collected by filtration. The crude product was redissolved in 30 mL of glacial acetic acid and the solution cooled in an ice/water bath. Concentrated sodium hydroxide solution was added dropwise until a pH of 5.5−6.0 was attained. The mixture was left to stand under an inert atmosphere for 16 h. The reprecipitated product **9** was collected by filtration and dried in vacuo; yield 1.25 g (7.21 mmol, 81%). IR: 3429 (m), 3325 (m, br), 2473 (w), 1694 (s), 1654 (s), 1613 (s, br), 1402 (s), 1329 (w), 1294 (m), 1255 (m), 655 (w), 637 (w), 611 (w), 453 (m) cm^{-1}. MS (*m*/*e*): 173 (M^+, 100). This material was used without further purification in subsequent steps.

Preparation of 8-Chloro-4*H*-bis[1,2,3]dithiazolo[4,5-*b*:5′,4′-*e*]pyridin-2-ium Chloride, [ClBPH][Cl], 10. This compound was prepared by two different methods. Route 1 (Scheme 1): 2,6-Diaminopyridine-3,5-dithiol (1.20 g, 6.93 mmol) and excess S_2Cl_2 (11 mL, 13.9 mmol) were stirred at reflux in 60 mL of chlorobenzene under an inert atmosphere for 16 h. The reaction mixture was cooled to room temperature and the (relatively pure) [ClBPH][Cl] collected by filtration, washed with 20 mL of methylene chloride and then 20 mL of acetonitrile, and dried in vacuo. Recrystallization of the purple-black powder was not possible due to its insolubility, but metathesis with $AgSbF_6$ (see below) afforded a pure hexafluorantimonate, yield 1.57 g (5.19 mmol, 75%), mp > 186 °C dec. IR: 3084 (vw), 2741 (vw), 1655 (w), 1624 (w), 1507 (m), 1328 (s), 1105 (m), 842 (vw), 831 (s), 761 (s), 721 (w), 708 (w), 665 (s), 630 (s), 519 (m), 501 (w), 480 (s) cm^{-1}. MS (*m*/*e*): 266 (M^+, 35), 265 ([M − H]$^+$, 92)]. Route 2 (Scheme 2): 2,6-Diaminopyridine (10.0 g, 91.6 mmol) and excess S_2Cl_2 (25 mL, 312 mmol) were stirred at reflux in 500 mL of dichloroethane under an inert atmosphere for 16 h. The reaction mixture was cooled to room temperature and the (highly impure) black powder collected by filtration, washed with 200 mL of hot chlorobenzene and then 200 mL of methylene chloride, and dried in vacuo; crude yield 29.02 g, whose IR spectrum was characteristic of [ClBPH][Cl]. Gallium trichloride (10.0 g, 56.8 mmol) was then added to a slurry of crude [ClBPH][Cl] (14.05 g, 46.5 mmol) in 150 mL of acetonitrile. The mixture was stirred for 30 min under an inert atmosphere to afford a deep turquoise solution. The solvent was removed by flash distillation and the deep red [ClBPH][$GaCl_4$] (**13**) dried in vacuo. The solid was washed with 3 × 150 mL of glacial acetic acid and the red, microcrystalline solid collected by filtration and dried in vacuo; yield 14.1 g (29.5 mmol, 64%). The product **13** was redissolved in 200 mL of acetonitrile, and to this was added 20 mL of pyridine to afford a dark purple precipitate of **10**. The powder was collected by filtration, washed with 2 × 50 mL of ethanol, and dried in air; yield 8.7 g (28.8 mmol, 97% from [ClBPH][$GaCl_4$]).

Preparation of 8-Chloro-4*H*-bis[1,2,3]dithiazolo[4,5-*b*:5′,4′-*e*]pyridin-2-ium Hexafluoroantimonate, [ClBPH][SbF6], 11. This compound was prepared by two different methods. Route 1: **10** (1.20 g, 3.97 mmol) and $AgSbF_6$ (1.47 g, 4.28 mmol) were stirred in 15 mL of SO_2 for 48 h to afford a turquoise solution with bronze microcrystals and a white precipitate of AgCl. The product was extracted 10 times with SO_2 and the solvent removed by evaporation. The product was washed with 40 mL of glacial acetic acid and dried in air to yield a bronze, microcrystalline product, yield 1.40 g (2.78 mmol, 70%). Crystals of **11** for analytical purpose were obtained by recrystallization from hot glacial acetic acid; mp > 250 °C. UV−vis (CH_3CN): λ_{max} = 661 nm, log ϵ = 4.5. IR: 3259 (w), 1660 (w), 1548 (w), 1329 (s), 1103 (m), 1030 (w), 949 (w), 841 (s), 725 (w), 716 (w), 668 (s), 653

(46) Beard, C. D.; Baum, K.; Grakauskas, V. *J. Org. Chem.* **1973**, *38*, 3673.

(s), 637 (m), 558 (w), 522 (m), 472 (s) cm^{-1}. MS (*m*/*e*): 266 (M^+, 5), 265 ($[M - H]^+$, 34). Anal. Calcd for $C_5HClF_6N_3S_4Sb$: C, 11.95; N, 8.36. Found: C, 12.16; N, 8.50. Route 2: **10** (7.90 g, 26.1 mmol) and $AgSbF_6$ (9.88 g, 28.7 mmol) were stirred at gentle reflux in 150 mL of acetonitrile for 24 h to afford a deep turquoise solution and a white AgCl precipitate. The solution was suction filtered and the filtrate combined with 100 mL of chlorobenzene. The solution was concentrated to 50 mL on a rotary evaporator and the bronze, microcrystalline product collected by filtration, washed with 50 mL of chlorobenzene, and dried in air; yield 11.13 g (22.1 mmol, 85%). Materials prepared by either of routes 1 and 2 were of sufficient purity to be used in the synthesis of ClBP (**12**).

Synthesis of 8-Chlorobis[1,2,3]dithiazolo[4,5-*b*:5′,4′-*e*]pyridine, ClBP, 12. A solution of Proton Sponge (0.99, 4.66 mmol) in 2 mL of methylene chloride was added, via syringe, to a stirred solution of **11** (1.00 g, 1.98 mmol) in 15 mL of acetonitrile. A blue/gray precipitate formed immediately. After 5 min the product **12** was collected by filtration, washed with 20 mL of acetonitrile, and dried in vacuo; yield 0.52 g (1.95 mmol, 98%); mp > 250 °C dec. IR: 1407 (w), 1267 (m), 1097 (w), 862 (vw), 830 (s), 754 (s), 732 (m), 641 (m), 525 (m), 488 (w), 469 (m) cm^{-1}. MS (*m*/*e*) 265 (M^+, 82). Recrystallization was not possible due to the insolubility of the product. Crystals suitable for X-ray structural determination were grown by layered diffusion. A solution of **11** (0.100 g, 0.20 mmol) in 5 mL of acetonitrile was added slowly to an unstirred solution of Proton Sponge (0.125 g, 0.58 mmol) in 10 mL of methylene chloride. Green/black needles of the solvate $[ClBP]_2 \cdot CH_2Cl_2$ grew at the interface of the two solutions; mp > 250 °C dec. IR: 1405 (vw), 1265 (m), 1103 (w), 864 (vw), 832 (s), 751 (s), 729 (vs), 639 (s), 536 (m), 523 (s), 490 (m), 461 (s) cm^{-1}. This solvate was characterized crystallographically.

Preparation of 8-Chloro-4-methyl-4*H*-bis[1,2,3]dithiazolo[4,5-*b*:5′,4′-*e*]pyridin-2-ium Trifluoromethanesulfonate, [ClBPMe][OTf]. Methyl trifluoromethanesulfonate (1.4 mL, 12.4 mmol) was added, via syringe, to a stirred slurry of **12** (2.58 g, 9.7 mmol) in 80 mL of anhydrous diethyl ether. The reaction mixture was stirred for 12 h, and the red microcrystals of [ClBPMe][OTf] were collected by filtration, washed with 2 × 30 mL of anhydrous ether, and dried in vacuo; crude yield 3.70 g (8.6 mmol, 89%). The material was recrystallized from hot acetonitrile (1.0 g per 60 mL). The recrystallized yield varied from 60% to 70% (from crude material); mp > 250 °C dec. IR: 1516 (w), 1491 (s), 1424 (s), 1347 (s), 1277 (s), 1237 (vs), 1171 (s), 1120 (m), 1057 (m), 1025 (vs), 985 (w), 924 (w), 874 (w), 832 (m), 768 (vs), 717 (w), 674 (s), 637 (s), 612 (w), 575 (w), 540 (w), 515 (m), 477 (s) cm^{-1}. Anal. Calcd for $C_7H_3ClF_3N_3O_3S_5$: C, 19.56; H, 0.70; N, 9.77. Found: C, 19.80; H, 0.56; N, 9.86.

Preparation of 8-Chloro-4-methyl-4*H*-bis[1,2,3]dithiazolo[4,5-*b*:5′,4′-*e*]pyridin-3-yl, ClBPMe, 6a (R = Me). Solid decamethylferrocene (0.670 mg, 2.05 mmol) was added to a solution of [ClBPMe][OTf] (0.860 g, 2.00 mmol) in 15 mL of degassed acetonitrile, under an inert atmosphere, for 45 min. Green/brown microcrystals of **6a** (R = Me) were collected by filtration, washed with 3 × 15 mL of acetonitrile, and dried in vacuo; yield 0.535 g (1.90 mmol, 95%). Recrystallization from hot, degassed, dichloroethane (0.150 g, 0.53 mmol, in 30 mL) afforded green/bronze needles; yield 0.115 g (0.41 mmol, 77% from crude material); mp > 250 °C dec. IR: 1455 (s), 1400 (vw), 1240 (s), 1194 (m), 1045 (m), 972 (m), 794 (s), 745 (s), 679 (s), 655 (s), 592 (s), 511 (s), 476 (w), 458 (m) cm^{-1}. Anal. Calcd for $C_6H_3N_3S_4Cl$: C, 25.66; H, 1.08; N, 14.96. Found: C, 25.72; H, 0.86; N, 15.11.

Preparation of 8-Chloro-4-ethyl-4*H*-bis[1,2,3]dithiazolo[4,5-*b*:5′,4′-*e*]pyridin-2-ium Trifluoromethanesulfonate, [ClBPEt][OTf]. Ethyl trifluoromethanesulfonate (2.0 mL, 0.018 mol) was added, via syringe, to a stirring slurry of **12** (2.48 g, 9.34 mmol) in anhydrous diethyl ether (170 mL) under a nitrogen atmosphere. The reaction mixture was stirred for 4 days, and the red, microcrystals of [ClBPEt][OTf] were collected by filtration, washed with anhydrous diethyl ether (2 × 30 mL), and dried in air; crude yield 3.70 g (8.3 mmol, 89%). The product was recrystallized from hot glacial acetic acid (1.0 g in 100 mL and then concentrated to 50 mL); yield 1.368 g (3.08 mmol); mp > 250 °C dec. IR: 1520 (m), 1363 (m), 1269 (m), 1241 (m), 1189 (w), 1169 (w), 1082 (w), 1026 (s), 891 (w), 821 (w), 793 (w), 765 (vs), 667 (s), 637 (vs), 609 (w), 573 (w), 553 (w), 515 (m), 477 (vs) cm^{-1}. Anal. Calcd for $C_8H_5ClF_3N_3O_3S_5$: C, 21.64; H, 1.14; N, 9.47. Found: C, 22.00; H, 1.01; N, 9.63.

Preparation of 8-Chloro-4-ethyl-4*H*-bis[1,2,3]dithiazolo[4,5-*b*:5′,4′-*e*]pyridin-3-yl, ClBPEt, 6b (R = Et). Solid decamethylferrocene (0.387 g, 1.18 mmol) was added to a solution of [ClBPEt][OTf] (0.507 g, 1.14 mmol) in 25 mL of degassed CH_3CN, and the mixture stirred under an inert atmosphere for 1 h. Green/brown microcrystals of **6b** (R = Et) were collected by filtration, washed with acetonitrile (3 × 15 mL), and dried in vacuo; yield 0.333 g (1.13 mmol, 99%). Recrystallization from hot, degassed, dichloroethane (0.152 g, 0.52 mmol, in 50 mL) afforded green/bronze needles, yield 0.083 g (0.28 mmol, 54% from crude material), mp > 250 °C dec. IR: 1495 (w), 1421 (w), 1313 (w), 1217 (m), 1180 (w), 1083 (w), 1073 (w), 1003 (m), 789 (vs), 743 (s), 686 (vs), 658 (m), 596 (s), 524 (w), 509 (m), 495 (w), 466 (s) cm^{-1}. Anal. Calcd for $C_7H_5N_3S_4Cl$: C, 28.51; H, 1.71; N, 14.25. Found: C, 28.70; H, 1.79; N, 14.32.

Preparation of 8-Chloro-4-propyl-4*H*-bis[1,2,3]dithiazolo[4,5-*b*:5′,4′-*e*]pyridin-2-ium Trifluoromethanesulfonate, [ClBPPr][OTf]. Propyl trifluoromethanesulfonate (5.0 g, 0.026 mol) was added, via syringe, to a stirred slurry of **12** (1.75 g, 6.58 mmol) in anhydrous diethyl ether (20 mL) under an inert atmosphere. The reaction mixture was stirred at room temperature for 4 days, and the red, microcrystals of [ClBPPr][OTf] were collected by filtration, washed with anhydrous diethyl ether (2 × 10 mL), and dried in air; crude yield 2.0 g (4.36 mmol, 66%). The crude product was dissolved in acetonitrile, filtered, and evaporated. The evaporate was recrystallized from hot glacial acetic acid (1.0 g in 50 mL); yield 1.37 g (2.99 mmol, 68% from crude yield); mp > 250 °C dec. IR: 3158 (w), 1554 (w), 1518 (w), 1342 (s), 1244 (s), 1180 (m), 1109 (w), 1028 (s) 969 (w), 925 (w), 849 (w), 839 (m), 767 (vs), 748 (w), 671 (m), 635 (vs), 573 (w), 522 (w), 513 (m), 476 (s) cm^{-1}. Anal. Calcd for $C_9H_7ClF_3N_3O_3S_5$: C, 23.60; H, 1.54; N, 9.18. Found: C, 23.82; H, 1.34; N, 8.94.

Preparation of 8-Chloro-4-propyl-4*H*-bis[1,2,3]dithiazolo[4,5-*b*:5′,4′-*e*]pyridin-3-yl, ClBPPr, 6c (R = Pr). Solid decamethylferrocene (0.23 g, 0.71 mmol) was added to a solution of [ClBPPr][OTf] (0.30 g, 0.65 mmol) in 15 mL of CH_3CN and the mixture stirred, under an inert atmosphere, for 1 h. The resulting green/brown microcrystals of **6c** (R = Pr) were collected by filtration, washed with acetonitrile (3 × 15 mL), and dried in vacuo; yield 0.17 g (0.55 mmol, 84%). Recrystallization from hot, degassed, dichloroethane (0.17 g, 0.55 mmol, in 20 mL) afforded green/bronze needles, yield 0.095 g (0.31 mmol, 56% from crude material), mp > 250 °C dec. IR: 1493 (w), 1422 (w), 1313 (w), 1273 (w), 1216 (s), 1081 (m), 970 (m), 891 (w), 795 (vs), 742 (vs), 687 (s), 655 (m), 627 (m), 594 (w), 529 (m), 509 (s), 468 (s), 458 (m) cm^{-1}. Anal. Calcd for $C_8H_7N_3S_4Cl$: C, 31.11; H, 2.16; N, 13.60. Found: C, 31.13; H, 2.16; N, 13.70.

EPR Spectra. X-Band EPR spectra were recorded at ambient temperature using a Bruker EMX-200 spectrometer; samples of the radicals were dissolved in degassed CH_2Cl_2. Hyperfine coupling constants were obtained by spectral simulation using Simfonia[47] and WinSim. The sweep width (SW), Lorentzian/Gaussian (L/G) ratio, and line width (LW) used in the simulation of the ClBPMe spectrum are provided in the caption to Figure 5.

Density Functional Calculations. All DFT calculations on ClBP and ClBPH were run on PC workstations using the B3LYP DFT method, as contained in the Gaussian 98W suite of programs.[48] Geometries were optimized using the 6-31G** basis set, within the constraints of C_{2v} symmetry.

(47) WinEPR Simfonia, Bruker Instruments, Inc., Billerica, MA.

Cyclic Voltammetry. Cyclic voltammetry was performed using a PINE Bipotentiostat, model AFCClBP1, with scan rates of 50−100 mV s^{-1} on solutions of [ClBPH][SbF_6] and [ClBPR][OTf] (R = Me, Et, Pr) in CH_3CN (dried by distillation from P_2O_5) containing 0.1 M tetra-*n*-butylammonium hexafluorophosphate. Potentials were scanned with respect to the quasi-reference electrode in a single-compartment cell fitted with Pt electrodes and referenced to the Fc/Fc^+ couple of ferrocene at 0.38 V vs SCE.[49] The $E_{pa}-E_{pc}$ separations of the reversible couples were within 10% of that of the Fc/Fc^+ couple.

X-ray Measurements. X-ray data for all three structures were collected with monochromated Mo Kα radiation on diffractometers using CCD detection. The three room-temperature data sets (Table 3) were collected at the University of Arkansas on a Rigaku Mercury diffractometer, while the 25 K data set was collected at the University of Toledo on a Siemens SMART unit using a prototype helium cryostat.[50] Crystals were mounted onto glass fibers with silicone or epoxy. The structures were solved using direct methods and refined by full-matrix least-squares which minimized $\sum w(\Delta F^2)^2$. The ClBPMe crystal cracked into two domains upon cooling; the larger component (92%) was well defined, while the data for the second one (8%) were relatively poor. A refinement on both components converged to 8.3% (52° cutoff in 2θ). A better model was obtained by refining on only those reflections that originated from the dominant component.

Magnetic Susceptibility Measurements. Magnetic susceptibilities were measured over the temperature range 5−380 K on a George Associates Faraday balance operating at 0.5 T.

Conductivity Measurements. Single-crystal (along the needle axis) conductivities were measured in a four-probe configuration, with in-line contacts made using silver paint. Conductivity was measured in a custom-made helium variable-temperature probe using a Lake Shore 340 temperature controller. A Keithley 236 unit was used as a voltage source and current meter, and two 6517A Keithley electrometers were used to measure the voltage drop between the potential leads in the four-probe configuration.

Band Calculations. Band electronic structure calculations were performed with the EHMACC suite of programs[51] using the Coulomb parameters of Baasch, Viste, and Gray[52] and a quasi-split valence basis set adapted from Clementi and Roetti;[53] numerical values are tabulated elsewhere.[54] The off-diagonal elements of the Hamiltonian matrix were calculated with the standard weighting formula.[55] Atomic positions were taken from the crystallographic data.

Acknowledgment. We thank the Natural Sciences and Engineering Research Council of Canada (NSERCC), the U.S. Office of Basic Energy Sciences, Department of Energy (Grant No. DE-FG02-97ER45668), the Office of Naval Research (Contract No. N00014-99-1-0392), and the Arkansas Science and Technology Authority for financial support. We also thank the NSERCC for a postgraduate scholarship to L.B.

Supporting Information Available: Details of X-ray crystallographic data collection and structure refinement and tables of atomic coordinates, bond distances and angles, anisotropic thermal parameters, and hydrogen atom positions for ClBPR (R = Me, Et and Pr) (CIF). This material is available free of charge via the Internet at http://pubs.acs.org.

JA026118S

(48) Frisch, M. J.; Trucks, G. W.; Schlegel, H. B.; Scuseria, G. E.; Robb, M. A.; Cheeseman, J. R.; Zakrzewski, V. G.; Montgomery, J. A., Jr.; Stratmann, R. E.; Burant, J. C.; Dapprich, S.; Millam, J. M.; Daniels, A. D.; Kudin, K. N.; Strain, M. C.; Farkas, O.; Tomasi, J.; Barons, V.; Cossi, M.; Cammi, R.; Mennucci, B.; Pomelli, C.; Adamo, C.; Clifford, S.; Ochterski, J.; Petersson, G. A.; Ayala, P. Y.; Cui, Q.; Morokuma, K.; Malick, D. K.; Rabuck, A. D.; Raghavachari, K.; Foreman, J. B.; Cioslowski, J.; Ortiz, J. V.; Stefanov, B. B.; Liu, G.; Fox, D. J.; Keith, T.; Al-Laham, M. A.; Peng, C. Y.; Nanayakkara, A.; Wong, M. W.; Andres, J. L.; Gonzalez, C.; Head-Gordon, M.; Repogle, E. S.; Pople, J. A. *Gaussian 98*, revision A6; Gaussian, Inc.: Pittsburgh, PA, 1998.
(49) Boeré, R. T.; Moock, K. H.; Parvez, M. *Z. Anorg. Allg. Chem.* **1994**, *620*, 1589.
(50) Hardie, M. J.; Kirschbaum, K.; Martin, A.; Pinkerton, A. A. *J. Appl. Cryst.* **1998**, *31*, 815.
(51) EHMACC, Quantum Chemistry Program Exchange, program number 571.
(52) Basch, H.; Viste, A.; Gray, H. B. *Theor. Chim. Acta* **1965**, *3*, 458.
(53) Clementi, E.; Roetti, C. *At. Data Nucl. Data Tables* **1974**, *14*, 177.
(54) Cordes, A. W.; Haddon, R. C.; Oakley, R. T.; Schneemeyer, L. F.; Waszczak, J. V.; Young, K. M.; Zimmerman, N. M. *J. Am. Chem. Soc.* **1991**, *113*, 582.
(55) Ammeter, J. H.; Bürgi, H. B.; Thibeault, J. C.; Hoffmann, R. *J. Am. Chem. Soc.* **1978**, *100*, 3686.